

Scattering from reflective diffraction gratings: the challenges of measurement and verification

Monika Kroneberger^a, Andreas Mezger^a, Jean-Baptiste Volatier^a
^aOHB System AG, Manfred-Fuchs-Straße 1, 82234 Weßling, Germany

ABSTRACT

The accurate simulation of straylight is essential for the verification of the contrast requirements in optical instruments. In a spectrometer, the scattering from reflective gratings is hardly understood and difficult to characterize while contributing significantly to the overall system straylight and reduction of the spectrometer contrast. In this article we present an experimental setup for, and measurement results from, the characterization of the bidirectional scattering distribution function (BSDF) of a grating in the scope of the FLORIS project of the ESA FLEX Mission. The grating is an Engineering Model and will be subject to further optimization. Measurement of the BSDF showed approximately a Harvey-Shack profile parallel to the grating grooves, consistent with a dominant contribution from roughness scatter and minor distinctive features. Moreover, we observed distinct straylight peaks out of the diffraction plane, which are called “satellites”. The main challenges in the measurement of grating BSDFs arise from the near angle limit, the determination of the instrument signature and the selection of the appropriate sampling (2D or 3D). Theoretical analysis has been performed to investigate the influence of, and limitations introduced by, the measurement setup combined with the convex curvature of the grating. The next step is to introduce these measured BSDFs into straylight simulation. We have done that by fitting appropriate functions to the measured BSDF and defining them in the optical analysis software ASAP as a user-defined BSDF.

Keywords: optical gratings, BSDF, straylight, Albatross TT scatterometer, straylight requirement

1. INTRODUCTION

Straylight requirements for the FLORIS gratings are defined as equivalent surface roughness [1]. The required BSDF (Bi-directional Scatter Distribution Function) is approximated by a Harvey-Shack function (see Figure 1-1) at the peak of the diffraction order is designed to operate. The acceptance of the grating requires the measured BSDF to be lower than the specified BSDF.

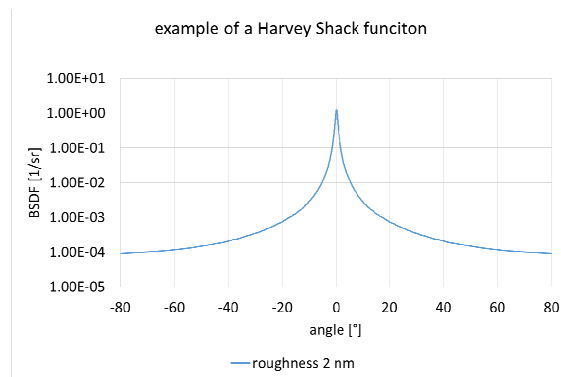


Figure 1-1. Example of a BSDF approximated by a Harvey-Shack function for a mirror with 2nm roughness at 532 nm wavelength

The BSDF function measured by a scatterometer, such as the Albatross TT, is expressed by the following equation, corresponding to the geometry illustrated in Figure 1-2:

$$\text{BSDF}(\theta_i, \theta_s, \phi_s) = \frac{dP_s(\theta_s, \phi_s)}{d\Omega_s P_i \cos \theta_s}$$

The incident angle is referred by θ_i . θ_s and ϕ_s refer to the azimuthal and tangential scattering angle, P_i is the power incident on the sample and P_s is the scattered power collected by the detector in the solid angle $d\Omega_s$.

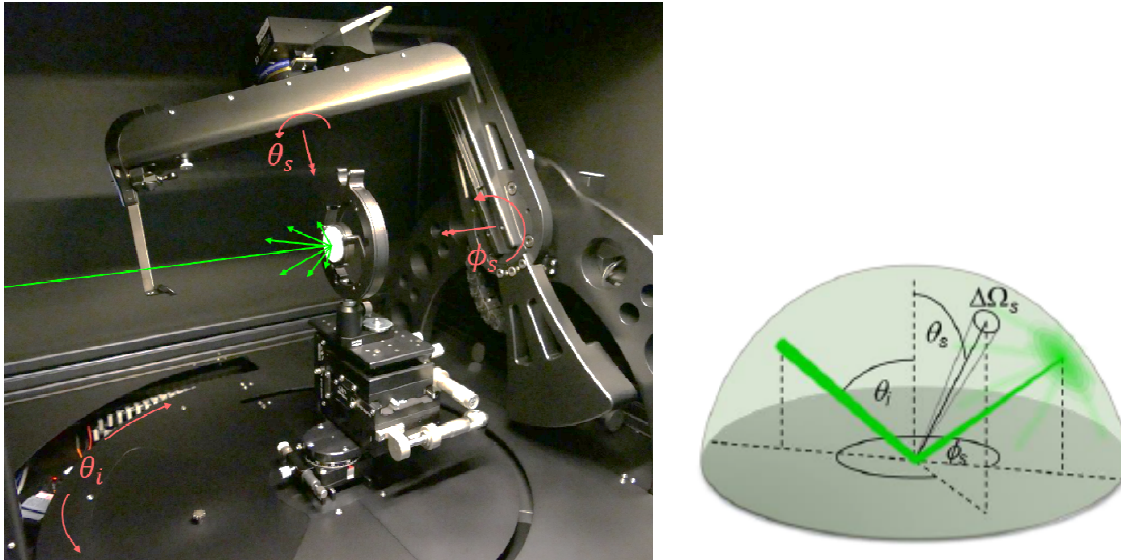


Figure 1-2. Albatross TT and its measurement geometry (right figure extracted from the manual courtesy of Fraunhofer IOF)

This setup allows measurement of a 3-dimensional BSDF by varying θ_s and ϕ_s for a given incidence angle. The properties of the Albatross TT are summarized in Table 1. The near angle limit is defined by the angle from the center of a reflection peak, where the scatterometer is able to determine between instrument signature and straylight from the test sample. The near angle limit depends on the optical geometry of the scatterometer and the sample under test. The instrument signature is the BSDF of the scatterometer itself.

Table 1. Albatross TT properties.

Albatross TT	
Wavelength	532 or 1064nm
θ_i	-90° to +90°
ϕ_s	-90° to +90°
θ_s	-180° to +180°
Angular resolution	< 0.02°
Dynamic range	13 orders of magnitude
Near angle limit	0.1°
Sample size	< 100 × 100mm

2. MEASUREMENT OF CURVED SAMPLES

The Offner type gratings used in the FLORIS spectrometers are aberration optimized to improve the optical performance of the spectrometers. To measure curved gratings, we need to focus the scatterometer. Focusing is achieved by configuring the scatterometer's "beam preparation unit".

Once focused, we cannot use the setup without a sample with an appropriate curvature. This makes direct measurement of the scatterometer's signature without a sample impossible. In our case, we are interested in the near angle signature, which includes aberration and straylight from the scatterometer optics. There are two ways to obtain the near angle signature in a focused configuration:

Indirect method

- 1) First the signature measurement is done in a standard configuration (appropriate for flat samples) as shown in Figure 2-4 (left, blue line).
- 2) Then the signature is simulated including straylight and aberration in the same configuration to reasonable agreement with the measured signature as shown in Figure 2-2 (left) and Figure 2-4 (left). A critical aspect is then to model correctly the straylight properties of all components.
- 3) The simulation is re-done in the focused configuration (appropriate for the curvature of interest). As the scattering properties of the optical elements do not change and we simulated the sample as a perfect mirror, our simulation in Figure 2-2 (right) should be close to the real instrument signature for a convex sample curvature of 100mm.

Direct method

It is also possible to replace the sample by a mirror with the same curvature and negligible scattering behavior. The BSDF we then measure is very close to the real instrument signature (see Figure 2-4 right).

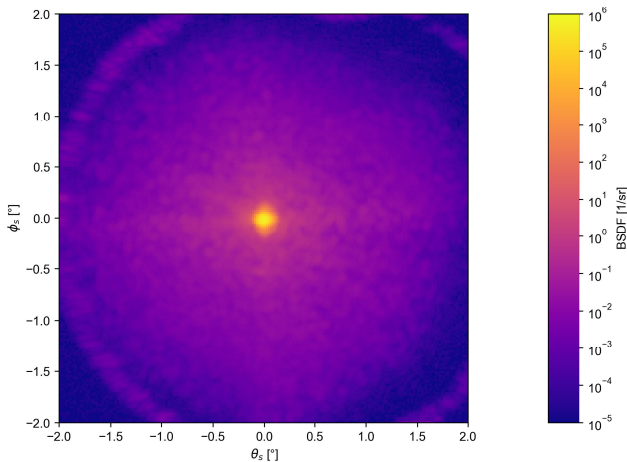


Figure 2-1. Measured scatterometer near angle signature for the nominal system.

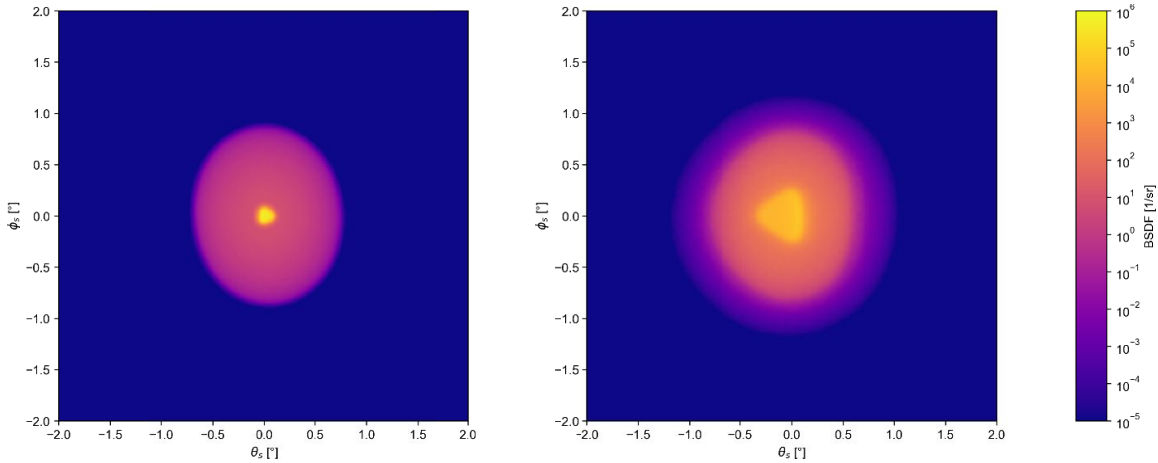


Figure 2-2. Left: Simulated scatterometer near angle signature for the nominal configuration. This simulated irradiance pattern is in good agreement with the measurements illustrated in Figure 2-1. Right: a focused configuration adapted for a convex sample with 100mm radius of curvature.

The simulated near angle signature is a combination of three contributors: optical aberrations in the scatterometer (or in the combination of scatterometer and sample in the focused case), scattering from the instrument itself and clipping by the detector field of view. Examining central, horizontal cuts extracted from Figure 2-2 (left and right) we can reduce the simulation results to two-dimensional plots, which we can compare directly to our 2D measurements in Figure 2-4.

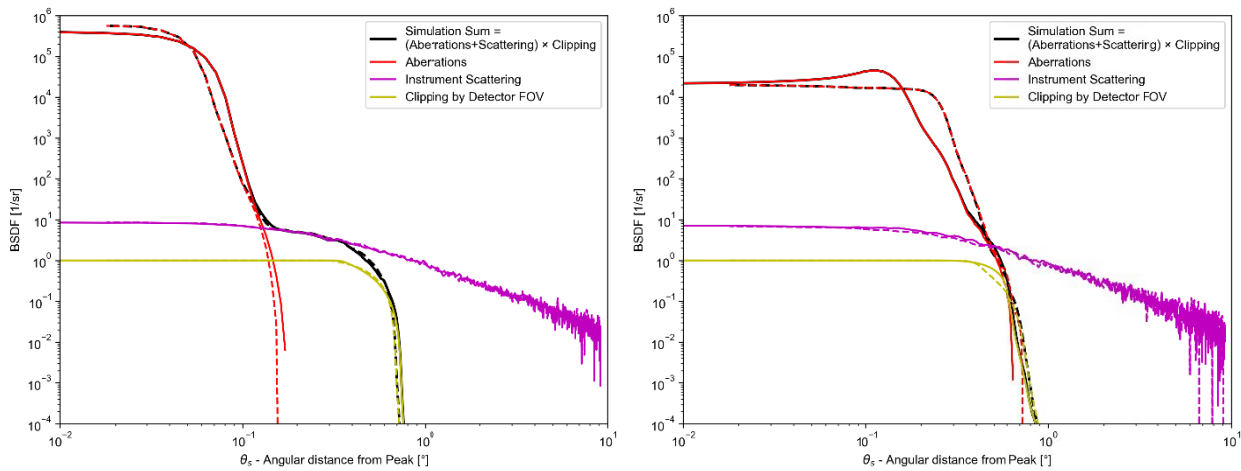


Figure 2-3. Simulated contributors to the scatterometer near angle signature with nominal focused configuration (left) and focused configuration adapted to a convex sample with a 100mm radius of curvature (right).

Figure 2-3 demonstrates that in the focused case, the aberration increases reciprocally with the convex radius of curvature of the test sample. In the focused configuration, the near angle limit occurring between 0.5° and 0.7° instead of 0.1° in the nominal configuration as shown in Figure 2-3 (left). These results also illustrate a limitation of the measurement setup; namely, the impossibility of measuring scattering close to the specular direction (within the near angle limit) due to the width of the signature function.

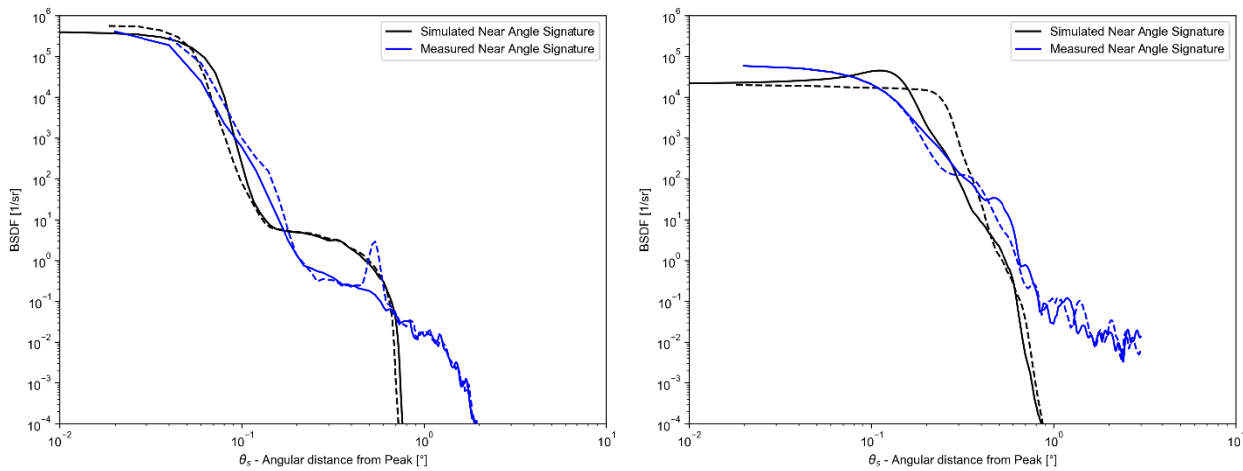


Figure 2-4. Comparison of measured near angle signature and simulation results from Figure 2-3. (Left) nominal configuration, (right) focused configuration adapted for a convex sample with 100mm radius of curvature.

Figure 2-4 shows a comparison between measured and simulated near angle signature. The simulation of the nominal configuration does not match the measurements, especially between 0.1° and 0.6° , where the scattering at the scatterometer optics is dominating the near angle signature (see purple line in Figure 2-3). For our straylight simulation, we used the parameters given in [3] for the Albatross TT, however we expect that these values are somewhat pessimistic and that the Albatross TT system exhibits lower straylight levels.

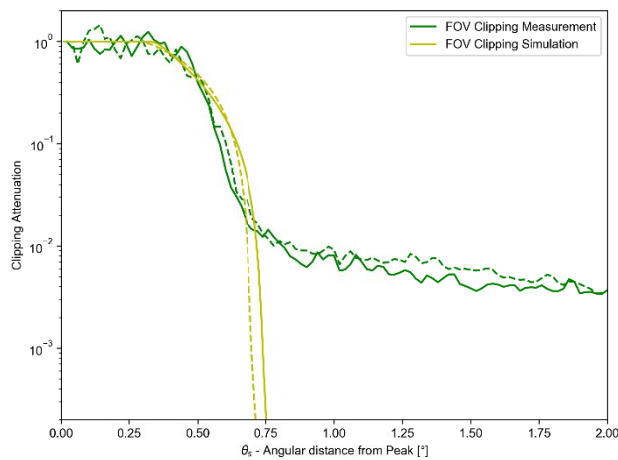


Figure 2-5. Comparison between simulated detector FOV clipping and measurement.

In the region between 0.7° and 0.9° on Figure 2-4 the simulated near angle signature drops to zero because of the detector FOV clipping. The optic between the adjustable aperture and the detector of the Albatross TT limits the field of view (FOV) of the detector. The measurements in Figure 2-5 show that the detector is not completely blind behind its theoretical FOV. We could not find the cause with final evidence, but effects like straylight or ghosting inside the detector optics are potential candidates. As the detector FOV does not change in any focused configuration of the measurement setup, the simulation can be improved by using the measured FOV clipping data instead of the theoretical prediction. In addition, the scattering parameters representative of Albatross TT optical surfaces do not depend on the focus configurations. These parameters are the only uncertain contributors to the near angle signature, all variations to the signature as a function of focus are of a geometrical nature and can be simulated by raytracing.

As previously mentioned there is a second way of obtaining the near angle signature: by replacing the sample with a mirror having the same curvature. If the mirror's scattering behavior is negligible and much lower than the sample, the near angle signature can be directly measured. For a comparison with our grating measurement we used an off-the-shelf silicon lens with the same radius of curvature as the grating. It acts as a mirror at the measurement wavelength of 532nm. To reduce the scattering at the lens surface we selected a spot on the lens which exhibited the lowest scatter. Even if the used lens might have a non-negligible surface roughness, we used it to obtain an upper limit for the instrument signature. Furthermore, we showed in Figure 2-3 that optical aberrations dominate the instrument signature in the angular range of interest. Figure 2-6 shows the BSDF around the -1st order diffraction peak of the grating and the instrument signature BSDF obtained by substituting the silicon lens for the grating. To account for the different reflectivity and the grating efficiency, we scaled the signature BSDF to give the same value at the peak.

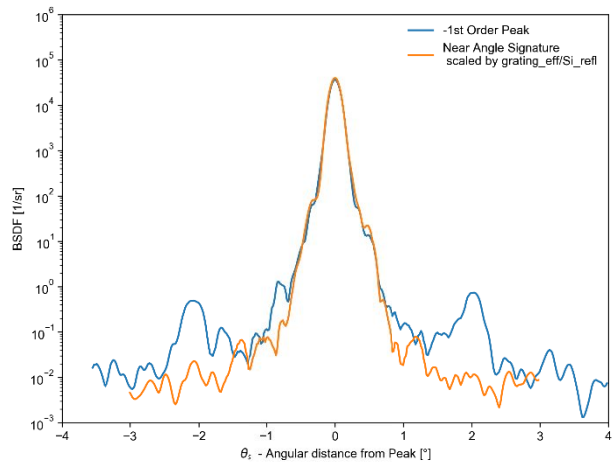


Figure 2-6. Comparison of -1st order peak scattering of a convex grating and measured instrument signature, making use of a silicon lens with same curvature. The FWHM of the signature is determined by the aberration of the scatterometer plus the sample curvature. Contributions below 10⁰ 1/sr are determined by the scattering properties.

3. MEASUREMENT RESULTS

Measuring the 2D BSDF (Bi-directional Scattering Distribution Function) of the breadboard grating and comparing it to calculated BSDF for several roughnesses fitted with a Harvey-Shack formula [4],[5] shows that the grating scattering is lower than an equivalent 2 nm RMS roughness scattering BSDF above 1° scatter angle. The straylight measurements of the breadboard / EM phase will be used as a starting point for a possible optimization of the flight model.

However as indicated in Figure 3-1 two features, stand out of the envelope curve. From the 2D plot it is difficult to determine whether the features are point-like or ring-like in the angular domain.

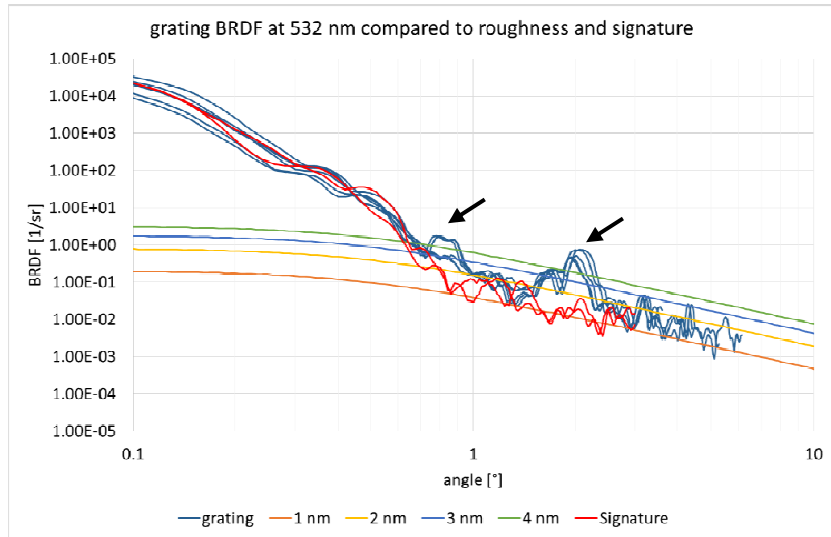


Figure 3-1. Grating BSDF compared to roughness BSDF, features of interest are indicated by arrows.

Using the Albatross TT, we are able to measure a 3D scan (Figure 3-2), indicating that the features form scattering rings and other peaks around high order diffraction peaks. The complete scatter map for the angles $\pm 150^\circ$ and $\pm 10^\circ$ show that many of the peaks are outside the field of view of the spectrometer.

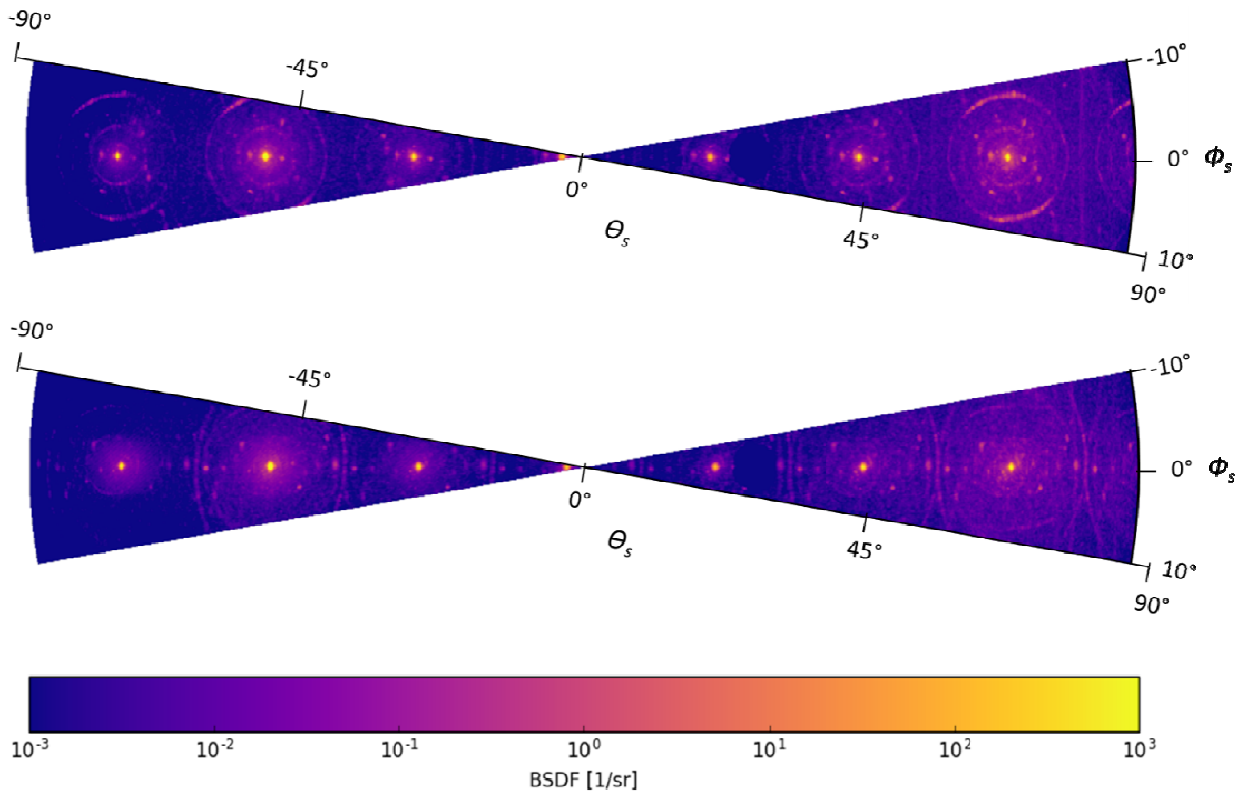


Figure 3-2 3D BSDF maps for two different locations on the grating for scatter angles between $\pm 150^\circ$ and $\pm 10^\circ$. In the purple disk around $17.4^\circ \theta$ the scatterometer cannot measure straylight because the detector optic obscures the illumination.

The measured results emphasize the importance of 3D scanning when measuring a grating's BSDF, restricting the measurement to 2D would produce different results depending on the alignment of the measurement plane with the

diffraction plane. For example Figure 3-3, depicts a close-up of the -1st order diffraction peak and its vicinity. With a 2D measurement, the two satellite peaks would only be observable within a narrow range of cut angles. Furthermore, at each location on the grating, the BSDF can be different (see Figure 3-2) and dependent upon the selected 2D measurement direction. The angle of the cut is determined by the line through the nominal diffraction peaks of the grating and is therefore not freely chosen by the operator, whereas the position of the satellite is a local property of the grating.

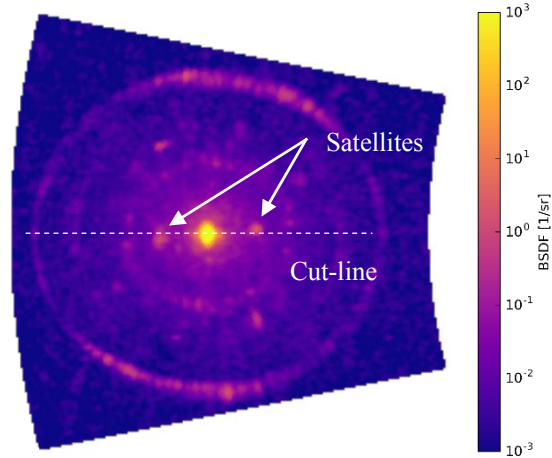


Figure 3-3 Close-up of the -1st order peak (range $\varphi_S = -13^\circ$ to 13° and $\theta_S = -43.4^\circ$ to -25.4°) feature showing the angle of the satellites.

We also show that the measured scatter pattern depends upon the region of the grating that is tested. The variation results from local surface irregularities. We hypothesise that the satellites shown in Figure 3-3 arise from the photolithographic manufacturing process of the grating. False light in the holographic illumination setup may cause additional, faint grating patterns, which are later etched into the grating substrate. The resulting groove depth is accordingly much lower than the actual grating flanges. Depending on the holographic illumination setup, the additional grating patterns can have different orientations and grating frequencies and do not necessarily cover the entire grating aperture.

In general, the holographic manufacturing process is able to minimize these effects or even to selectively shift the superimposed gratings to regions with no impact. Therefore, a well-defined specification is mandatory. The grating used in this work is a holographic standard convex spherical grating used in an Engineering Model phase of the FLEX FLORIS programme. The holographic signature is quite typical. For the manufacturing of the Flight Model grating, the holographic setup will be optimized in an iterative procedure to generate gratings with optimum performance (diffraction efficiency, polarization sensitivity and straylight) based on the findings of the EM phase.

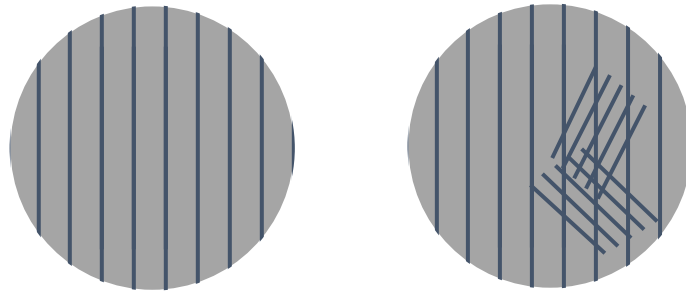


Figure 3-4. Schematic of a perfect grating on the left and a grating illuminated by an illumination system suffering from false light.

To test the hypothesis that the observed scattering is due to superimposed grating structures, we simulated a synthetic grating and its far field scatter pattern by computing the power spectral density using a Fourier transform. We attempted to reconstruct the measured straylight features in Figure 3-3 by testing a composition of various superimposed gratings. Figure 3-5 shows a promising candidate grating structure. It is composed of a nominal grating profile superimposed with three additional gratings: two linear and one concentric. Zooming on the 1st order peak of the nominal derived far field we obtain in Figure 3-6 (left).

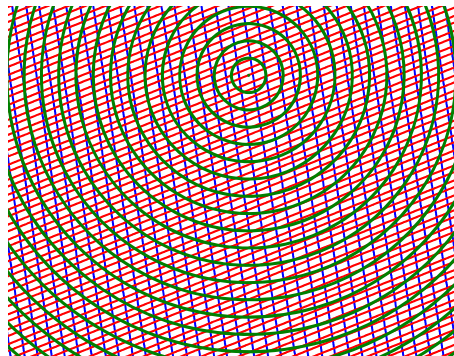


Figure 3-5. Synthetic, additional superimposed grating patterns used to investigate qualitatively the induced diffraction artifacts (so called satellites).

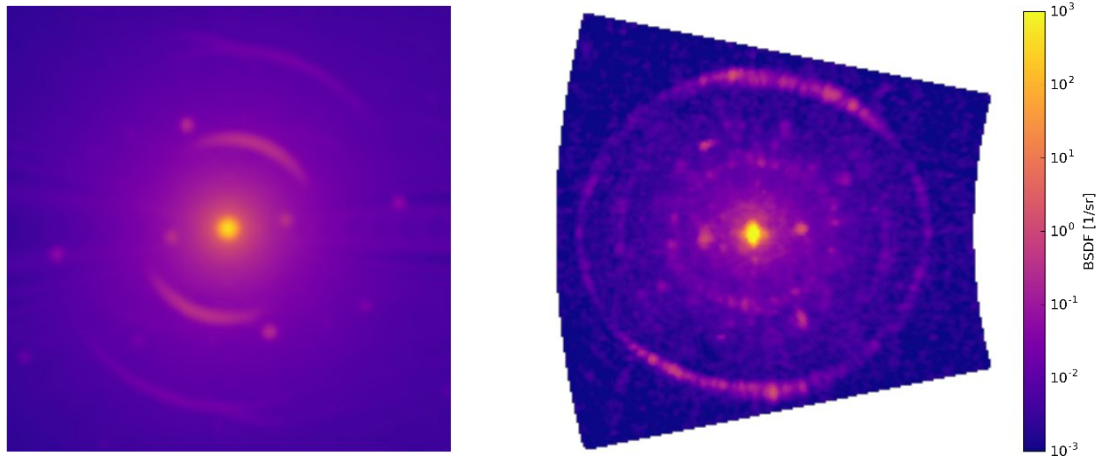


Figure 3-6. Qualitative simulated far field diffraction from a synthetic grating profile with superimposed additional gratings from Figure 3-5 in arbitrary units (left). Measured BSDF of -1^{st} order peak in the range $\phi_S = -13^\circ$ to 13° and $\theta_S = -43.4^\circ$ to -25.4° (right)

The comparison of the simulated diffraction features in Figure 3-6 (left) with the measurement (right) shows that it is possible that these artifacts are indeed caused by grating structures superimposed on the nominal grating.

4. EVALUATION OF ANALYTICAL BSDF FOR SIMULATION

Simulating the straylight of the system, including the measured BSDF of the grating, would be possible by using the tabulated data of the measurement. However, the interpolation would slow down the simulation drastically, so this is not a viable option. We chose to fit the satellites with Gaussian functions and the smooth scattered light with a Harvey Shack function. For one of the measured positions on the grating the six most intense satellites were fitted.

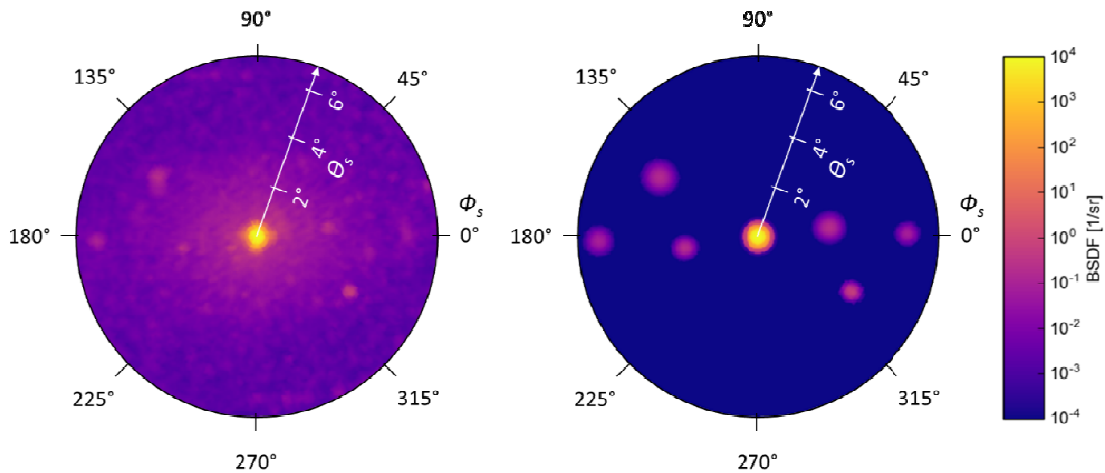


Figure 4-1: Measured BSDF of -1^{st} order peak and satellites of the grating, with a near angle limit of ca. 0.7° (left). Fitted BSDF of -1^{st} order peak and satellites (right).

Analogous to [1], we compared the underlying scatter in Figure 4-1 (left) to Harvey Shack functions with different rms roughness equivalents (see Figure 3-1). A Harvey Shack function corresponding to 3 nm rms roughness at a wavelength of 532 nm covers the maximum envelope for BSDF below 1° scatter angle without taking the satellites into account (indicated with an arrow in Figure 3-1).

The six Gaussian satellites were defined as user functions in ASAP and a USERBSDF was created using the satellites and the Harvey Shack function for the base scatter. The resulting BSDF is shown in Figure 4-2.

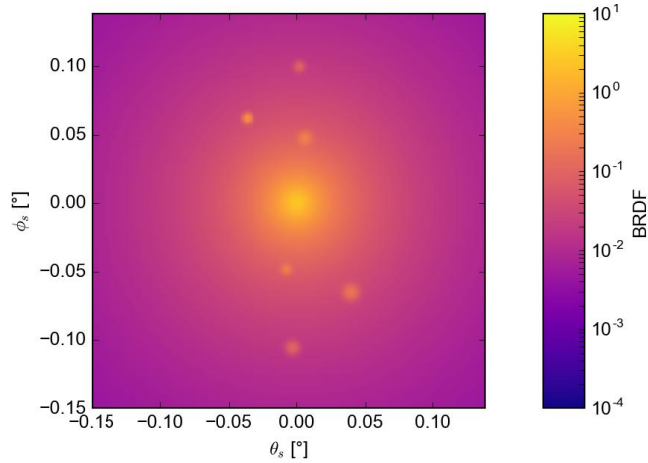


Figure 4-2. BSDF in ASAP for the six dominating satellites and basic scatter of the grating

A simple test case was simulated in ASAP to confirm that the resulting scattered irradiance distribution will present satellites. In this test case, the grating is illuminated by a slightly diverging beam and the direct light and straylight are detected on a sphere surrounding the grating and the source.

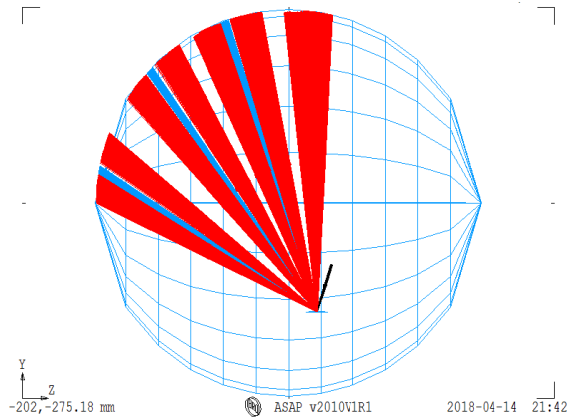


Figure 4-3. Simple test system: illumination of the grating and detection of the direct and scattered rays on a sphere around the grating and source.

As a result, an irradiance distribution normalized to the irradiance of the nominal diffraction peak is computed. As shown in Figure 4-4 and Figure 4-5 the satellites are clearly reproduced for all diffraction orders. In Figure 4-4 the Harvey Shack function was not included in the grating BSDF, while in Figure 4-5 both effects are included. These simulations are carried out with only 3000 incident rays (hence the poor statistics).

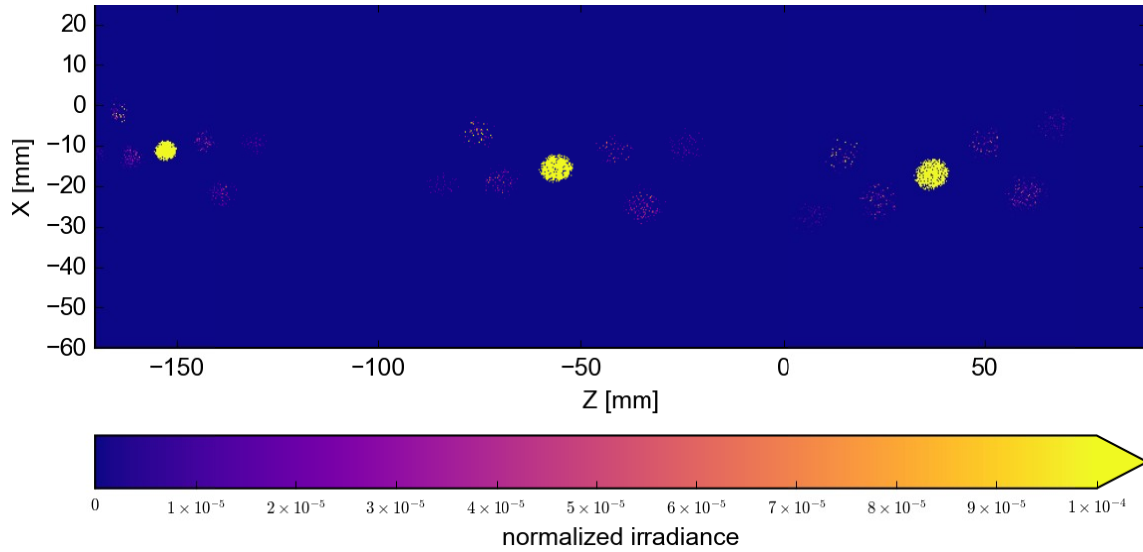


Figure 4-4: Irradiance distribution on the sphere normalized to the irradiance of the nominal diffraction order.

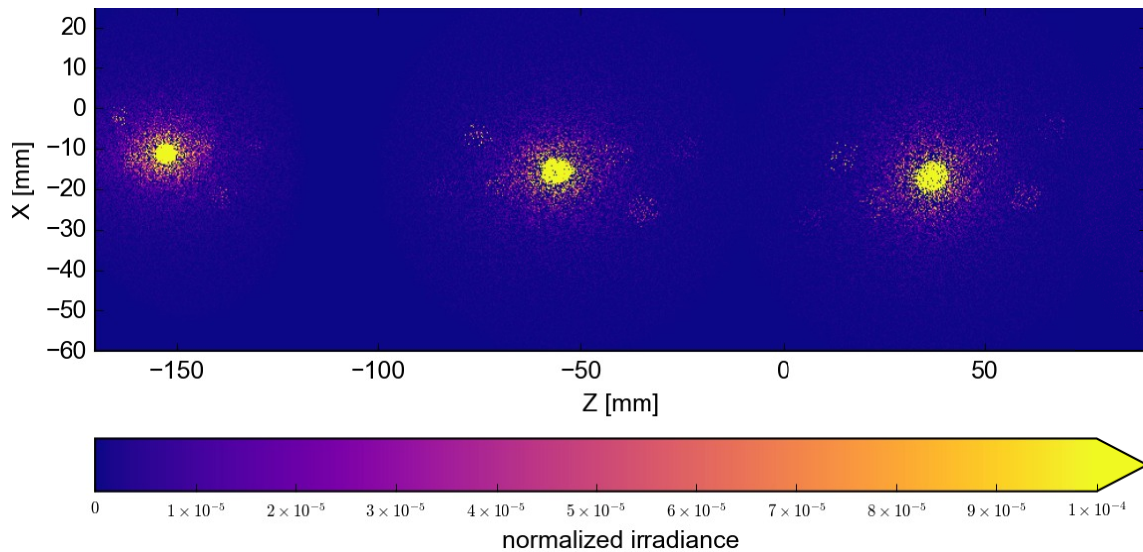


Figure 4-5: Irradiance distribution on the sphere normalized to the irradiance of the nominal diffraction order. BSDF includes Harvey Shack scatter function. Satellites are marked by the arrows.

5. SIMULATION RESULTS WITH ANALYTICAL GRATING BSDF

The BSDF was finally applied to the simulation of the complete spectrometer system. The simulation takes into account roughness scatter on all optical elements, but contamination and ghosting are not considered. The wavelength 500 nm was chosen (the lowest wavelength of the detection range). Figure 5-1 shows the resulting straylight incident on the detector of the spectrometer on top of the image of the point source. In addition to the halo around the image of the point source (top center of Figure 5-1) the satellites of the grating simulated as scatter are clearly visible. In a nominal scene they will add to spectral and spatial straylight because they are displaced from the image of the source in both directions. The relative irradiance with respect to the nominal light is of the order 10^{-6} and will normally not disturb a scene significantly. However, for high-contrast scenes (for example with clouds and earth surface) the nominal illumination can vary by one to two orders of magnitude from line to line and cause the relative irradiance to be significantly increased. As straylight requirements for spectrometers can be in the range of 10^{-4} we conclude that the satellites of

gratings can lead to non-compliance of the instrument to the requirements. The presented simulations are performed exemplarily and are valid only for a small subaperture of the grating, where we measured the underlying BSDF. As the BSDF may depend on the position at the grating surface the final image can be smeared out, or even more satellites could appear.

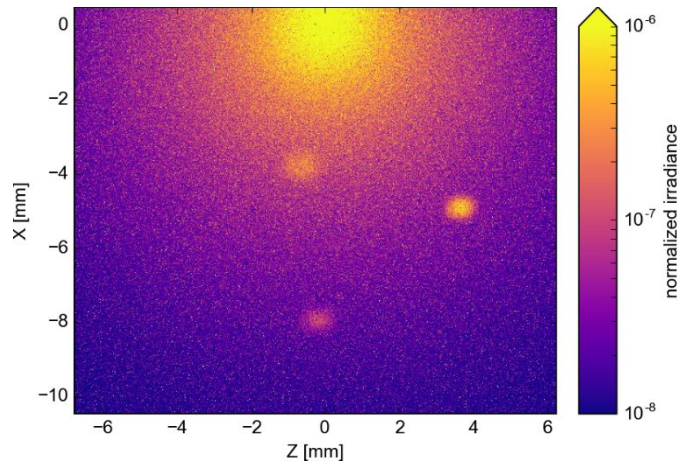


Figure 5-1: Roughness scatter distribution on the detector for a point source of 500 nm in the middle of the spectrometers slit.

6. REQUIREMENT DEFINITION FOR GRATING SUPPLIER

Measurement and simulation of the grating BSDF have shown that the satellites can travel through the system and cause straylight on the detector. The challenge now is to define requirements for the grating to minimize these satellites. The holographic manufacturing process allows minimization of the amplitude of the superimposed gratings, and even adjustment of their period. In that way, we can influence the location of the satellites at the detector plane. Because superimposed gratings are a matter of optimization and their relation to satellites is predictable, we propose to define an exclusion zone for satellites (red rectangle in Figure 6-1). Furthermore, we propose to keep the existing requirement definition of a maximum equivalent rms roughness in the form of a maximum BSDF template as illustrated in Figure 6-1. If some satellites still occur inside the specified exclusion zone, their intensity is required to be below the specified BSDF template. Outside the exclusion zone, the satellites can be ignored.

In order to achieve an independently verifiable requirement, we propose to define the exclusion zone and BSDF template in the angle space. The grating of a spectrometer is located at the pupil of the system. Therefore, we can exploit the Fourier relationship between the pupil and image space.

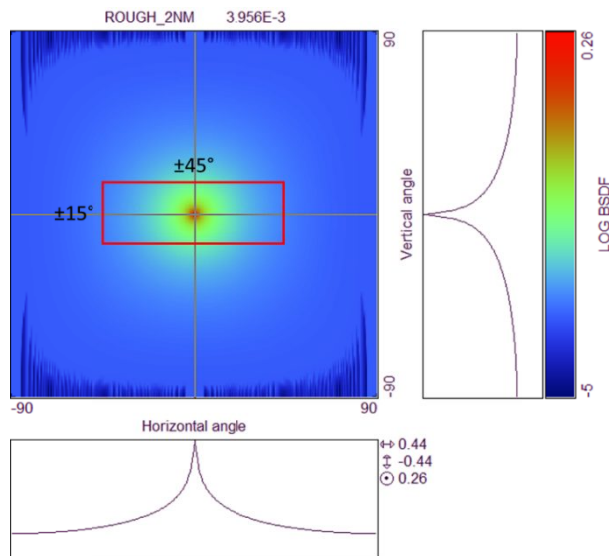


Figure 6-1: BSDL template for grating scatter and exclusion zone for satellites. (Dark lines are artefacts from translation into rectangular angle space)

The exclusion zone shall take into account the spectral and spatial limits of the detector, because the diffraction pattern as shown in Figure 5-1 shifts across the detector plane with different image points in the slit and different wavelengths. The scatterometer illuminates only a small spot of less than 1 mm diameter on the grating. When changing the position of this spot on the gratings surface, we observed a variation of the satellite position and intensity as an effect of surface irregularities as described in chapter 3. We need to consider this during the verification of our requirement. An adequate number of measurement positions and a consistent averaging of the results is required to correctly predict the straylight performance on system level, where the complete clear aperture of the grating is illuminated simultaneously.

7. CONCLUSION

We have shown the importance of characterizing BSDL with 3D scanning methods when studying highly anisotropic components such as gratings. The setup used in this article is capable of such measurements and is therefore insensitive to misalignment between the scanning plane and the diffraction plane that other measurement setups would have.

Proper care was taken to characterize the scatterometer signature, as the use with convex samples do not allow a direct measurement of the signature. In particular, we investigated determination of the near angle limit in our measurements, because of its inverse relationship with the radius of curvature of the grating. Simulations of the optical path showed that aberrations are the main cause of a degraded near angle limit.

A standard, convex spherical, blazed grating was used for measurements that showed anisotropic features. These features are caused by superimposed grating patterns on sub-apertures of the nominal grating. These grating patterns are probably produced by false light in the illumination optics used in the production of the grating structure itself. The level of these effects is negligible for the performance of standard spectrometers, but of significance for space and other high-end applications. Therefore, the production of holographic gratings for high-end applications require a sophisticated optimization process, taking into account all relevant straylight aspects.

Fitting the measured BSDL with analytical functions (Gaussian peaks and Harvey Shack functions), a BSDL of the grating for straylight simulation was defined. Our simulation shows, that the satellites can have significant influence on the image at the detector. We propose a modification of the straylight requirements for gratings, specifying a BSDL template and an exclusion zone for satellites within a certain angular range, which corresponds to the detector dimensions.

ACKNOWLEDGEMENTS

The authors acknowledge that this work is supported by an ESA funding through the FLEX Mission development.

REFERENCES

- [1] B. Harnisch, A. Deep, R.Vink, C. Coatantiec, "Grating Scattering BSDF and Imaging Performances", ICSO 2012, FP 156
- [2] Steiner, R., Pesch, A., Erdmann, L. H., Burkhardt, M., Gatto, A., Wipf, R., ... & van den Bosch, B. G. (2013, September). Fabrication of low straylight holographic gratings for space applications. In *Imaging Spectrometry XVIII* (Vol. 8870, p. 88700H). International Society for Optics and Photonics.
- [3] Finck, A., "Table top system for angle resolved light scattering measurement", dissertation at Fakultät für Maschinenbau der Technischen Universität Ilmenau, urn:nbn:de:gbv:ilm1-2014000214 (2014)
- [4] S.J. Wein, "Small-Angle scatter measurement", PhD Theses University of Arizona (1989)
- [5] M.G.Dittman, "Contamination scatter functions for stray-light analysis", *Proc. SPIE Vol. 4774* (2002)